

# Ionisation and dissociation of cometary gaseous organic molecules by solar wind particles I: Formic acid

S. Pilling<sup>1\*</sup>, A. C. F. Santos<sup>3</sup>, W. Wolff<sup>3</sup>, M. M. Sant'Anna<sup>3</sup>, A. L. F. Barros<sup>3</sup>  
G. G. B. de Souza<sup>2</sup>, N. V. de Castro Faria<sup>3</sup> and H. M. Boechat-Roberty<sup>4</sup>

<sup>1</sup>*Laboratório Nacional de Luz Síncrotron, Caixa Postal 6192, CEP 13084-971, Campinas, SP, Brazil.*

<sup>2</sup>*Instituto de Química, Universidade Federal do Rio de Janeiro - UFRJ, Ilha do Fundão, CEP 21949-900, Rio de Janeiro, RJ, Brazil.*

<sup>3</sup>*Instituto de Física, Universidade Federal do Rio de Janeiro - UFRJ, Ilha do Fundão, Caixa Postal 68528, CEP 21941-972, Rio de Janeiro, RJ, Brazil.*

<sup>4</sup>*Observatório do Valongo, Universidade Federal do Rio de Janeiro - UFRJ, Ladeira Pedro Antônio 43, CEP 20080-090, Rio de Janeiro, RJ, Brazil.*

Received / Accepted

## ABSTRACT

In order to simulate the effects of energetic charged particles present in the solar wind colliding with the cometary gaseous formic acid molecule (HCOOH), laboratory experiments have been performed. The absolute ionisation and dissociation cross sections for this molecule interacting with solar wind particles were measured employing fast electrons in the energy range of 0.5 to 2 keV and energetic protons with energies varying from 0.128 to 2 MeV. Despite the fact that both projectiles lead to a very similar fragmentation pattern, differences in the relative intensities of the fragments were observed. Formic acid survives about 4-5 times more to the proton beam than to the energetic electron collision. The minimum momentum transfer in the electron impact case was estimated to be 3-38% larger than the minimum momentum transfer observed with the equivelocity protons. The UV photodissociation rates and half-lives for HCOOH are roughly closer to the values obtained with energetic electrons. It is consequently important to take electron impact data into account when developing chemical models to simulate the interplanetary conditions.

**Key words:** comets: general - molecular process - molecular data - Sun: solar wind - astrochemistry

## 1 INTRODUCTION

To the present date, about 50 molecules have been detected in comets. In particular, the glycine precursor molecule, formic acid (HCOOH), has been detected in several comets including comet C/2001 Q4 (Neat), C/2004 Q2 (Machholz) (Biver et al. 2005) and comet C/1995 O1 (Hale-Bopp) (Bockelée-Morvan et al. 2000), which have shown a formic acid abundance ( $[\text{HCOOH}]/[\text{H}_2\text{O}]$ ) up to 0.09 % at 1 AU from the Sun. These cometary molecules are highly exposed to the solar radiation (photons and particles) which induce several physical and chemical reaction processes, like ionisation and molecular dissociation.

Comets consist of blocks of ice, mainly H<sub>2</sub>O, CO, and CO<sub>2</sub> molecules, and dust with a typical size of 0.1-10 km. According to the Safronov theory most comets were formed in the Uranus-Neptune region and were dynamically expelled to form the Oort cloud, a large spherical cloud with a radius from 10<sup>4</sup> to 10<sup>5</sup> AU surrounding the Sun (Safronov 1969; Mumma et al. 1993). The to-

tal number of comets is approximately 10<sup>12</sup>, and their expected total mass is roughly 100 Earth masses. A much smaller number of comets,  $\sim 10^9$ , are located in the Kuiper belt at 50-500 AU (Weissman 1991). Perturbations caused by the planets and nearby stars make some comets move towards the inner solar system. Ices evaporate and pick up dust at small heliocentric distances. Their flow is not gravitationally bound, and effects of the solar radiation and wind are responsible for the spectacular phenomena of the coma, dust and plasma tails.

The atomic and molecular ions released by the dissociation processes contribute to the alternative and efficient astrochemical evolution process of complex molecular synthesis, since some ion-molecule reactions do not have an activation barrier and are also very exothermic (Largo et al. 2004, Woon 2002, Pilling et al. 2005). These simple ions interact further with other ions to produce more and more complex molecules (Herbst & Leung 1996).

The formic acid molecule has been also observed in several other astronomical sources such as protostellar ices NGC 7538:IRS9, chondritic meteorites (Briscoe & Moore 1993), dark molecular clouds (Ehrenfreund & Schuttle 2000; Ohishi et al. 1992

\* E-mail: spilling@lnls.br

and references therein) and regions associated with stellar formation (Zuckerman, Ball & Gottlieb 1971; Winnewisser & Churchwell 1975; Liu et al. 2001, 2002). Fragmentation of the formic acid molecule by soft X-rays, present in star-forming regions, has recently been studied under laboratory conditions using synchrotron radiation (Boechat-Roberty, Pilling & Santos 2005).

This paper is the first in a series of experimental studies in an attempt to simulate the interaction between electrons and protons from the solar wind with cometary gaseous organic molecules. Formic acid is not the most abundant molecule in the organic cometary inventory. However, it plays an important role in the chemistry of biomolecules like amino acids (Woon et al. 2002; Mendoza et al. 2004.). Crovisier et al. (2004) have calculated some upper limits for the simplest amino acid, glycine ( $\text{NH}_2\text{CH}_2\text{COOH}$ ), from radio spectroscopic observations of comet C/1995 O1 (Hale-Bopp).

Two other reasons were also decisive for the choice of  $\text{HCOOH}$  for this experimental study. First, it offers the possibility of making a comparison between the interaction of energetic particles and stellar X-rays photons with molecules, as previously studied (Boechat-Roberty, Pilling & Santos 2005). The second reason is the low mass resolution of the time-of-flight system used in the proton impact experiment, which prevents a reliable mass spectrum measurement of highly hydrogenated molecules. We plan to circumvent this limitation in the near future, making feasible studies involving hydrogen-rich and abundant molecules like methane ( $\text{CH}_4$ ), methanol ( $\text{CH}_3\text{OH}$ ), ethane ( $\text{CH}_3\text{CH}_3$ ), ethanol ( $\text{C}_2\text{H}_5\text{OH}$ ), dimethyl-ether ( $\text{CH}_3\text{OCH}_3$ ), acetic acid ( $\text{CH}_3\text{COOH}$ ), acetaldehyde ( $\text{CH}_3\text{CHO}$ ) and acetonitrile ( $\text{CH}_3\text{CN}$ ) among others.

A short review of solar wind properties is presented in the next section along with a discussion on the electron and proton flux. In the following sections, we present the experimental results on the ionisation and fragmentation of the formic acid molecule upon interaction with fast electrons and protons. The two experimental setups which have been used are described in section 3. In section 4, we present the results obtained for impact of both energetic particles with the gaseous formic acid including the kinetic energy released by ionic fragments, the momentum exchange with the projectiles, and the determination of the absolute cross sections, dissociation rates and half-lives. In section 5, final remarks and conclusions are given.

## 2 SOLAR WIND COMPOSITION AND INTERACTION WITH COMETARY GAS

The solar wind (or even the stellar wind) is formed by the hydrodynamical expansion of the outer shell of the solar atmosphere, the corona. This rarefied plasma region which is exposed to the strong solar gravity, is permeated by magnetic fields. The corona is heated by magnetic hydrodynamical wave (MHD) propagation, reaching temperatures of about  $2 \times 10^6$  K. Due to magnetic reconnections and annihilations, energetic charged particles like electrons, protons and alpha particles ( $\text{He}^{++}$ ) are ejected from the solar corona and interact with planetary atmospheres and comets. The interaction between the solar wind and atomic and molecular medium (interplanetary matter) has drastic consequences, beyond the direct ionisation and dissociation process. Processes like charge transfer, X-ray fluorescence and bremsstrahlung emission also occur as described in detail by Krasnopolsky, Greenwood & Stancil (2004) and references therein.

The mean solar wind velocity of 450 km/s corresponds to ion

**Table 1.** Averaged Properties of solar wind at 1 AU (adapted from Zirin 1988, Toptygin 1985 and Kroll & Trivelpiece 1973).

Properties	Quiet times	Disturbed times
Density <sup>†</sup>	$\sim 10$ ions/cm <sup>3</sup>	20-40 ions/cm <sup>3</sup>
Bulk speed	$\sim 450$ km/s (100-600 km/s)	$\sim 750$ km/s (700-900 km/s)
Ion temperature	$\sim 8 \times 10^4$ K	$\sim 3 \times 10^5$ K
Proton energy	$\sim 0.6$ keV	$\sim 3$ keV ( $1-10^4$ keV)
Electron energy	$\sim 0.3$ eV ( $0.1-10^4$ eV)	$\sim 1.5$ eV ( $0.1-10^4$ eV)
Magnetic field	$3 - 8 \times 10^{-5}$ G	$10 - 30 \times 10^{-5}$ G
Energy flux	$\sim 0.5$ erg/cm <sup>2</sup>	$\sim 15$ erg/cm <sup>2</sup>

<sup>†</sup> 95%  $\text{H}^+$ , 4%  $\text{He}^{++}$  and traces of C, N, O, Ne, Mg, Si and Fe ions

energy of  $\sim 1000$  eV/u (energy/atomic mass unit). The solar wind at high heliographic latitudes is emitted from coronal holes, and its velocity reaches roughly 750 km/s, corresponding to an energy of  $\sim 3000$  eV/u. The ion velocity decreases in the comet from the bow shock to the lower density regions, according to the Giotto measurements in the comet Halley (Goldstein et al. 1987). The elemental composition of the solar wind is generally similar to the solar composition (Grevesse & Sauval 1998). Relative element abundances in the slow ( $\sim 400$  km/s) and fast ( $\sim 750$  km/s) solar wind and in the solar photosphere are presented in Krasnopolsky, Greenwood & Stancil (2004) and von Steiger et al. (2000). The mean He/H ratio in the solar wind varies between 0.04 - 0.08, originating from different sources.

In Table 1 we present some solar wind averaged values taken from Zirin (1988), Toptygin (1985) and Kroll & Trivelpiece (1973). Near Earth, the velocity of the solar wind varies from 100-900 km/s. The average velocity is 450 km/s. Approximately 800 kg/s of material is lost by the Sun as ejected solar wind, a negligible amount compared to the Sun's light output, which is equivalent to about  $4.5 \times 10^9$  kg of mass converted to energy every second. The wind is believed to extend out to between 100 and 200 AU.

Measurements of the solar wind ion density (mainly  $\text{H}^+$ ,  $\text{He}^+$  and  $\text{He}^{++}$ ), as a function of distance from comet 1P/Halley, were performed by the Giotto spacecraft (Fuselier et al. 1991; Shelley et al. 1987), and by the Plasma Experiment for Planetary Exploration (PEPE) aboard the Deep Space 1 fly by of the comet 19P/Borrelly (Young et al. 2004). Those data have shown that the solar wind ions also capture electrons from cometary gases and induce some charge exchange processes with cometary gases like  $\text{H}_2\text{O}$  and  $\text{CO}_2$  (Greenwood et al. 2000).

Depending on the cometary gas production rate and solar wind conditions (and heliocentric distance), a bow shock or bow wave is generated in the mass-loaded solar wind, preceding it, slowing therefore the solar wind further, diverting the plasma flow around the dense inner coma, and heating the streaming plasma. In addition, a compression wave is formed. As the flow penetrates deeper into the coma, the neutral gas density becomes sufficiently high so that some ion-neutral particle collisions begin to dominate the fluid and the chemical characteristics of the flow (Härberli et al. 1995). The region where this occurs is termed collisionpause. Inside this region (roughly  $\sim 10^5$  km from the nucleus at Halley) two- and even three-body collisions begin to take place, setting off a wide range of complex physical and chemical process, including charge transfer, ion-neutral collisions and electron impact ionisation (Cravens 1997; Härberli et al. 1997). The charge transfer reduces the ionised component of the solar wind which presents a maximum where the ion mean free path begins to decrease rapidly (Gombosi 1987). Ion-neutral collisions lead to mo-

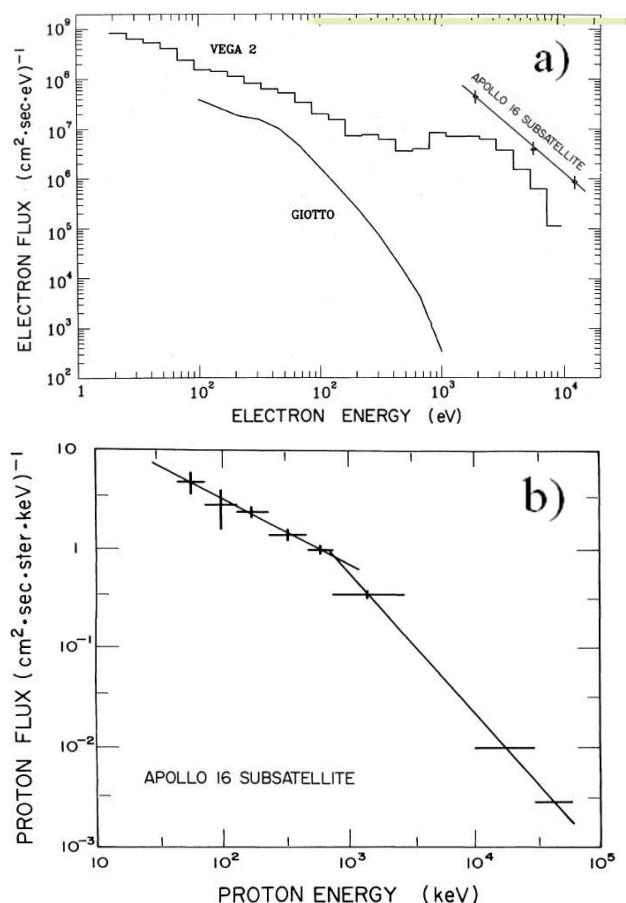


**Figure 1.** a) Electron fluxes in comet Halley measured by the Vega 2 (Gringauz et al., 1986) and by Giotto (d’Uston et al., 1989) and at lunar orbit measured by APOLLO 16 subsatellite (adapted from Lin, McGuire and Anderson, 1974). b) The proton energy spectrum due to solar wind at lunar orbit measured by APOLLO 16 subsatellite (Lin, McGuire and Anderson, 1974)

mentum exchange (Haberli et al. 1995, 1997) and formation of the collisionpause roughly at the point where the solar wind mean free path is comparable to the distance of the comet nucleus (Cravens 1997).

According to Rodgers & Charnley (2001) complex organic molecules cannot be synthesized in the coma and should originate from the nucleus. At lower altitudes, however, ionisation and dissociation processes may occur and these energetic radicals may react with each other or with the surrounding and abundant simple molecules (water, CO, CO<sub>2</sub>), promoting a slight increase in the molecular complexity of the region. This scenario may also have a small contribution on the formation of pre-biotic molecules, like the amino acids, since one of their precursor, the carboxyl radical (COOH) is produced in the fragmentation of formic acid, as we will see further.

In Fig. 1a we present the electron energy distribution (taken from Krasnopolsky, Greenwood & Stancil 2004) in comet Halley, measured at various distances from the nucleus by the Vega (Gringauz et al. 1986) and Giotto (d’Uston et al. 1989) probes together with the one obtained at lunar orbit measured by APOLLO 16 subsatellite (adapted from Lin, McGuire & Anderson 1974). The proton energy spectrum due to solar wind at lunar orbit measured

by APOLLO 16 subsatellite (Lin, McGuire & Anderson 1974) can be seen at Fig. 1b.

The mean energy of the solar wind protons is in the 1-2 keV range. The K-shell tightly bound electrons of the C and O atoms, for example, can be knocked off by solar wind protons. However, these K-shell ionisation cross sections are extremely low and their probability is much smaller than the fluorescence yield produced by solar x-rays.

### 3 EXPERIMENTAL SETUP

The formic acid gas target is first degassed through freezing, pumping and thawing cycles and then delivered in vapor form, through a thin needle, into the interaction region (volume defined by the gas intersection between the effusive jet and the projectile beam is about 1-3 mm<sup>3</sup>). The base pressure in the vacuum chamber was in the 10<sup>-8</sup>-10<sup>-6</sup> Torr range and during the experiment the chamber pressure was maintained below 10<sup>-5</sup> Torr. The pressure at the interaction region was estimated to be ~ 1 Torr (10<sup>16</sup> mols cm<sup>-3</sup>). These pressure values ensure a single collision regime. The measurements were made at room temperature.

#### 3.1 Proton impact

A tightly collimated monoenergetic proton beam with energies of 0.128, 0.2, 0.5, 1.0, 1.5 and 2.0 MeV is delivered by the 1.7 MV Tandem accelerator of the Federal University of Rio de Janeiro. The beam is charge analyzed by an electric field placed just before crossing, at right angles, an effusive jet of formic acid molecules. This is made in order to improve the charge state purity, since the proton beam can become partially neutralised due to the interactions with the residual gases present in the beam line. The emergent beam is recorded by a channeltron detector housed in a detection chamber downstream of the gas cell. A secondary electric field is applied after the intersection with molecular beam in order to separate the H<sup>0</sup> beam that performed single electron capture in interactions with the gas target (see Fig. 2b). For the higher projectile velocities, the direct ionisation process (the charge of the projectile does not change during the collision) is the dominant collision channel in the target ionisation, (Rudd et al. 1985a and 1985b). The average experimental proton flux was about 3 × 10<sup>5</sup> protons cm<sup>-2</sup> s<sup>-1</sup>.

The atomic and molecular ionic fragments ejected due to the interaction with the incident beam are accelerated by a two-stage electric field and detected by a channeltron detector. The time-of flight (TOF) spectrometer, running in the coincidence mode, is started by the detection of the proton beam and stopped by the ionic fragments extracted onto the TOF-detector.

The first stage of the electric field is produced by a plate-grid system subjected to a 130 V/cm electric field. The extracting electric field is raised up to 950 V/cm in order to assure the complete recoil collection. No differences are observed in the recoils yield, indicating that most fragments are ejected with small momenta. The limited mass resolution of the time-of-flight spectrometer does not allow for the separation of ionic fragments differing by 1 a.m.u.

#### 3.2 Electron impact

The electron impact apparatus has been described in details by Maciel, Morikawa & de Souza (1997). Briefly, a D.C. monoenergetic 0.5, 1.0 and 2.0 keV electron beam is produced and crossed with

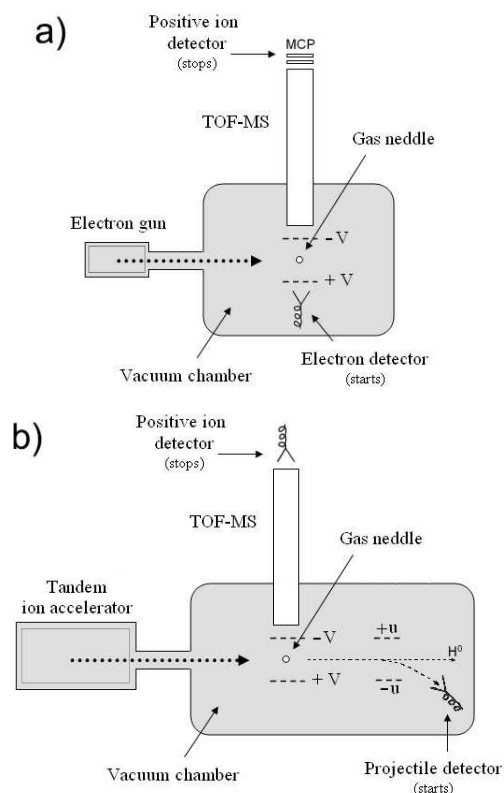


**Figure 2.** Experimental setup. a) high energy electron impact vacuum chamber. b) proton impact vacuum chamber.

the gaseous formic acid target jet. The fragments resulting from the collision are accelerated by a two-stage electric field and detected by a microchannel plate detector mounted in a chevron configuration. This detector provides the stop signals to the time-to-digital converter started by the signals from the secondary low energy electrons accelerated in the opposite direction. The first stage of TOF-detector consists of a plate-grid system with the primary beam passing through its middle with a 60 V/cm electric field. Ions with energies up to 5 eV have a 100 % collection efficiency. The averaged experimental electron flux was about  $10^{10}$ - $10^{11}$  electrons  $\text{cm}^{-2} \text{s}^{-1}$ .

A schematic diagram of both experimental setups is presented in Fig. 2. In the upper and bottom figures the vacuum chamber and the TOF-detector configuration for the electron and proton impact experiments are shown respectively.

#### 4 RESULTS AND DISCUSSION

Three formic acid electron impact mass spectra, obtained at 500, 1000 and 2000 eV impact energy are presented in Fig. 3a. The ionic fragments are labeled and indicated by arrows in the first spectrum. No significant changes are observed between the 0.5 - 2 keV electron impact experiments. For the sake of comparison, in Fig. 3b three mass spectra produced by proton impact with energies of 0.128, 1 and 2 MeV, respectively, are displayed. Again, only minor changes are observed between these spectra. The main difference between the proton and electron impact spectra is the peak broadening present in the proton impact spectra which reflects mainly the different mass resolution of the spectrometers.

A direct comparison between time-of-flight spectra, expressed

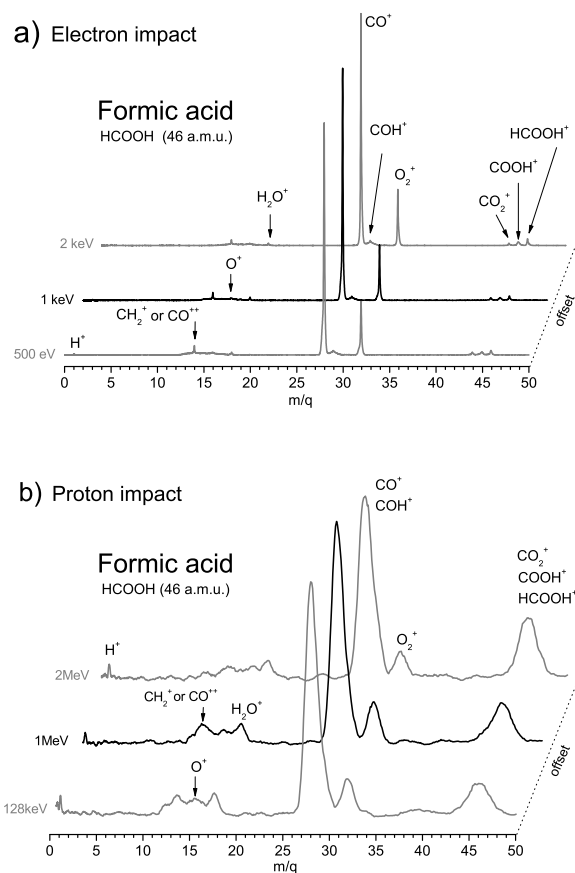


**Figure 3.** Time-of-flight mass spectrum of HCOOH molecule. a) recorded at 500 eV, 1 keV and 2 keV electron impact beam. b) recorded at 128 KeV, 1 MeV and 2 MeV proton impact beam.

in terms of mass over charge ratio, for the fragmentation of formic acid by 1.0 MeV protons and by roughly equivelocity 0.5 keV electron impact is presented in the Fig. 4. Despite the fact that both projectiles are leading to the same fragmentation pattern, we can clearly observe differences in the relative yield of the fragments (see Tables 2 and 3). The 0.5 keV electrons induce a stronger fragmentation of the formic acid molecules than the equivelocity 1.0 MeV protons. This observation is in direct accordance with the corresponding differences noted also in the rare gas target-electron and proton impact experiments (Melo et al. 2002) and has been suggested to arise from projectile charge effects. In the inset Fig. 4 (at right), we can see a deconvolution process of the highest mass peak obtained in the proton case, showing the contributions of fragments  $\text{CO}_2^+$ ,  $\text{COOH}^+$  and  $\text{HCOOH}^+$  superimposed with the peaks obtained in the electron case.

Since the electron and proton impact spectra have been obtained under different mass resolution conditions we have grouped some fragments (ex. CO group:  $\text{CO}^+ + \text{COH}^+$ ) to avoid uncertainties in the yield comparison. The fragments from each group are indicated by the upper arrows. The most significant differences are found in the yields of COO group ( $\text{CO}_2^+ + \text{COOH}^+ + \text{HCOOH}^+$ ) and  $\text{O}_2^+$ . The former present a yield 4 times higher than in the 1 MeV protons experiment and the latter about 2 times higher than in the experiment with 0.5 keV electrons.

Generally speaking, both projectile interactions lead to the

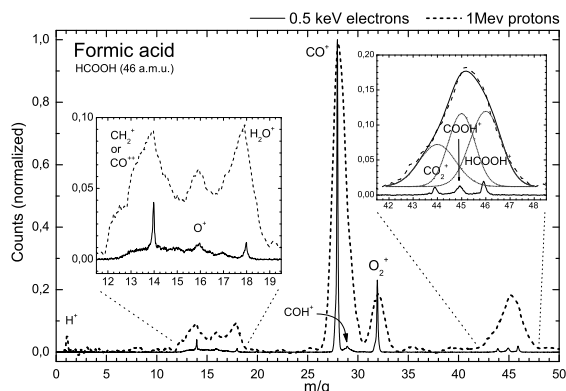


**Figure 4.** Comparison between mass spectra of formic acid fragments by 1 MeV protons and 0.5 keV electrons.

same formic acid fragments, but the overall relative intensities of the fragments are clearly distinct for each incident projectile. In addition, a comparison between both mass spectra conveys to some interesting observations. For both projectiles, the  $\text{CO}^+$  fragment dominates the spectra, though, in the proton impact case, this peak is clearly convoluted with the  $\text{HCO}^+$  peak.

Another interesting observation concerns the relative intensity of the  $\text{H}^+$ . In the proton case, it is roughly three times more intense than in the electron impact case. Whether this is a result of the spectrometer discrimination against high energetic fragments (due to its low mass,  $\text{H}^+$  takes most of the kinetic energy available in the dissociation process), or associated with different breakup mechanisms, is uncertain. On the other hand, the relative intensity of the  $\text{O}_2^+$  peak in the electron impact case overcomes by a factor of 2 the corresponding peak in the proton impact case.

#### 4.1 Partial ion yield and kinetic energy release

The Partial Ion Yield (PIY) or relative intensities for each fragment  $i$  was obtain by

$$PIY_i = \left( \frac{A_i}{A_t^+} \pm \frac{\sqrt{A_i} + A_i \times ER/100}{A_t^+} \right) \times 100\% \quad (1)$$

were  $A_i$  is the area of a fragment peak,  $A_t^+$  is the total area of the PEPICO spectrum. The  $ER = 2\%$  (in the electron impact) and  $10\%$  (in the proton impact) is the estimated error factor due to the data treatment.

Considering that the electric field in the interaction region is uniform, we can determine the mean kinetic energy released in the fragmentation process ( $U_0$ ) for each ionic fragment from the correspondent peak width, as suggested by Simon et al. (1991), Hansen et al. (1998) and Santos, Lucas & de Souza (2001)

$$U_0 = \left( \frac{qE\Delta t}{2} \right)^2 \frac{1}{2m} \quad (2)$$

where  $q$  is the ion fragment charge,  $E$  the electric field in the interaction region,  $m$  is the mass of the fragment, and  $\Delta t$  is the time peak width (FWHM) taken from time-of-flight mass spectra.

The relative intensities and mean kinetic energy release  $U_0$  (only for the electron impact case) are presented in tables 2 and 3, as a function of the incident energy for the electron and proton impact experiments, respectively. The water peak (18 a.m.u.) represents an

intrinsic recombination of some dissociation products of  $\text{HCOOH}$  already reported in the literature (Su et al 2000; Schwel et al 2002; Boechat-Roberty, Pilling & Santos 2005 and references therein).

The PIY for several fragments ejected in the dissociation process of the formic acid molecule in the 500-2000 eV electron energy range are displayed in Fig. 5. The PIY for the 70 eV electron impact data from NIST is also shown. The most abundant fragments,  $\text{CO}^+$  and  $\text{O}_2^+$ , exhibit almost a constant PIY in the electron energy above 500 eV. The yields of the  $\text{H}^+$ ,  $\text{H}_2\text{O}^+$ ,  $\text{HCO}^+$ ,  $\text{O}^+$  and  $\text{HCOOH}^+$  molecules are included in the same figure. The C group and the CO group are additionally shown, for further comparison with the proton impact data. In the high energy electron impact regime, we note that the PIY of the fragments remains basically unaltered, as the electron beam energy increases, with the exception of  $\text{COH}^+$  and the C group, which present a small variation with increasing projectile energy. The PIY obtained at 0.128-2 MeV proton impact for same fragments displayed in Fig. 5a, are shown in Fig. 5b. Despite some small fluctuations, the PIY of the fragments does not show any specific trend as a function of the proton energy.

In Fig. 5b the PIY for 0.128-2 MeV proton impact are shown for same fragments displayed in the Fig. 5a. Despite some small fluctuations the PIY of the fragments does not indicate any specific tendency as function of the proton energy.

A comparison between the averaged partial ion yield of the fragments of  $\text{HCOOH}$  released by 0.5 to 2 keV electron and 0.128 to 2 MeV proton beam impact could be seen in Fig. 6a. The main difference between the two impact regimens can be observed in the yield of COO group fragments. In the case of proton impact the yield of this group have shown roughly 5 times larger than the corresponding yield associated with the electron impact process. This corroborates the higher degree of dissociation promoted by the energetic electron collisions.

Searching for possible similarities we present, in the Fig. 6b, a comparison between partial ion yield of the fragments of  $\text{HCOOH}$  due to soft X-rays (290 eV) and VUV “pseudo-photons” (70 eV electron impact from NIST<sup>1</sup>). The degree of destruction of the  $\text{HCOOH}$  molecule is much larger in the soft X-rays case (Boechat-Roberty, Pilling & Santos 2005). Several fragments present a different pattern, as far as the PIY are concerned, in X-ray field when compared to the UV field. As an example, we could mention the large enhancement in the production of  $\text{CO}^+$  in the X Ray regime. The same is true for  $\text{O}^+$ ,  $\text{O}_2^+$  and  $\text{CH}_2^+$  fragments. On the other hand, the opposite behavior is observed with the  $\text{HCO}^+$  and  $\text{OH}^+$  fragments, which seem to be more efficiently produced by UV photons. This fact has been previously reported (Suto et al. 1988, Su et al. 2000 and Schwel et al. 2002).

The dissociation of the formic acid molecule by fast electrons and by soft X-rays shows several similarities. The survival of the  $\text{HCOOH}$  molecule, subjected to an incoming proton beam, was observed to be 6-8% while in the case of the fast electrons was about 2%, i. e., 3 to 4 times smaller. The reactive  $\text{COOH}^+$  fragment, also important in pre-biotic ion-molecule chemistry, shows a similar behavior along with the molecular ion  $\text{HCOOH}^+$ .

<sup>1</sup> The dissociation induced by 70 eV electrons is very similar to the dissociation induced by 21.21 eV (He I Lamp) photons. In both cases the ionisation occurs in the valence shell (see discussion in Lago et al 2004)

**Table 2.** Relative intensities (PIY) and kinetic energy  $U_0$  release by the fragments in the formic acid mass spectra, as a function of electron beam energy. Only fragments with intensity  $> 0.1\%$  were tabulated. The estimated experimental error was below 10%.

Fragments		PIY (%) / $U_0$ (eV)		
$m/q$	Attribution	500 eV	1000 eV	2000 eV
1	H <sup>+</sup>	0.79 / 1.5	0.47 / 1.1	0.76 / 0.81
12, 13, 14	C group <sup>a</sup>	11.6 / -	10.0 / -	8.89 / -
16	O <sup>+</sup>	3.1 / 1.1	3.3 / 1.1	3.4 / 1.1
17	OH <sup>+</sup>	1.2 / 0.85	0.95 / 0.85	0.96 / 0.85
18	H <sub>2</sub> O <sup>+</sup>	1.0 / 0.03	1.2 / 0.01	1.1 / 0.02
28	CO <sup>+</sup>	60.2 / 0.01	61.7 / 0.01	60.1 / 0.01
29	COH <sup>+</sup>	4.1 / 0.29	3.7 / 0.18	5.3 / 0.17
32	O <sub>2</sub> <sup>+</sup>	14.5 / 0.01	15.0 / 0.01	14.7 / 0.01
44	CO <sub>2</sub> <sup>+</sup>	0.83 / 0.02	0.92 / 0.01	0.74 / 0.01
45	COOH <sup>+</sup>	1.4 / 0.03	1.3 / 0.03	1.9 / 0.03
46	HCOOH <sup>+</sup>	1.3 / 0.01	1.4 / 0.01	2.0 / 0.01

<sup>a</sup> C<sup>+</sup> + CH<sup>+</sup> + CH<sub>2</sub><sup>+</sup> or CO<sup>++</sup>**Table 3.** Relative intensities (PIY) of fragments in the formic acid mass spectra, as a function of proton beam energy. Only fragments with intensity  $> 0.1\%$  were tabulated. The estimated experimental error was below 20%.

Fragments		PIY (%)					
$m/q$	Attribution	128 keV	200 keV	500 keV	1 MeV	1.5 MeV	2 MeV
1	H <sup>+</sup>	0.74	0.79	0.88	0.67	0.89	0.65
12, 13, 14	C group <sup>a</sup>	6.5	5.2	5.4	3.5	7.1	6.0
16, 17, 18	O group <sup>b</sup>	7.7	5.6	6.2	4.3	9.7	7.4
28, 29	CO group <sup>c</sup>	57.1	55.4	51.1	57.8	51.9	53.8
32	O <sub>2</sub> <sup>+</sup>	9.1	7.4	8.2	12.3	7.9	6.7
44, 45, 46	COO group <sup>d</sup>	16.8	25.6	27.9	21.4	22.3	25.3
44	CO <sub>2</sub> <sup>+</sup>	3.7	10.0	9.8	5.6	6.4	5.8
45	COOH <sup>+</sup>	7.9	9.4	11.2	8.7	8.0	13.0
46	HCOOH <sup>+</sup>	5.2	6.5	6.9	7.1	7.9	6.5

<sup>a</sup> C<sup>+</sup> + CH<sup>+</sup> + CH<sub>2</sub><sup>+</sup> or CO<sup>++</sup>; <sup>b</sup> O + OH + H<sub>2</sub>O; <sup>c</sup> CO<sup>+</sup> + COH<sup>+</sup>; <sup>d</sup> COO<sup>+</sup> + COOH<sup>+</sup> + HCOOH<sup>+</sup>

## 4.2 Projectile momentum exchange

It is accepted that the ionisation cross section, at high velocities, are the same for electrons and protons (Bethe 1930). In fact, within the first Born approximation, the total ionization cross section  $\sigma^+$  depends on the charge and the velocity of the incoming projectile according to the relationship

$$\sigma^+ \propto \frac{Z^2}{v^2} \ln v \quad (3)$$

being fundamentally the same for equivelocity electrons and protons, if the velocity is much larger than the binding energy of the active electron (Fano 1954).

In addition, the projectile dependence enters also through the  $P_{min}$ , the minimum momentum transfer. The value of  $P_{max}$  can be put to infinity without significantly affecting integrated cross sections because the integrand decreases at large  $P$ . The minimum momentum transfer occurs for scattering angles  $\theta$ , close to zero (Rudd et al., 1985)

$$P_{min}^2 = \frac{\varepsilon^2}{v^2} \left( 1 + \frac{\varepsilon^2}{2E_p} + \dots \right) \quad (4)$$

where  $\varepsilon = IP + E_{ej}$  is the transferred energy,  $IP$  is the formic acid ionization potential (11.33 eV),  $E_{ej}$  is the ejected electron energy,  $v$  is the projectile velocity and  $E_p$  is projectile energy.

As most ejected electrons are formed with  $E_{ej}$  close to zero, for equivelocity 2.0 MeV protons and 1.0 keV electrons, the cal-

culated difference in the minimum momentum transfer is only 3 % larger for electrons, being virtually the same ( $P_{min} \sim 0.047$  a.u.). As the projectile velocity decreases, the momentum transfer difference increases, reaching 38 % at  $v = 2.26$  a.u. (70 eV electron impact or 128 keV proton impact). The difference can be even higher due to the so-called trajectory effects: The Coulomb interaction between the projectile and the target nuclei will tend to accelerate and attract a negative projectile towards high electron densities, whereas a positive particle will be decelerated and repelled. In the case of proton impact, in addition, electron capture by the projectile becomes an important process at impact velocities close to the relevant target electron velocity further suppressing the direct ionisation channel further, as can be seen in Fig. 7c.

## 4.3 Absolute ionisation and dissociation cross section

The absolute cross sections for both ionisation and dissociation processes of organic molecules by solar wind are extremely relevant and essential as input for physico-chemical models (Haider & Bhardwaj 2005; Boice 2004; Rodgers et al. 2004) and molecular abundance models (Sorrell 2001). In those theoretical models, biomolecules are formed inside the bulk of icy grain mantles photoprocessed by starlight (ultraviolet and soft X-rays photons) and wind particles (protons, electrons, He<sup>+</sup>). As mentioned by Sorrell (2001), the principal uncertainty of these models comes from the uncertainty of the dissociation cross section values  $\sigma_d$ . Therefore

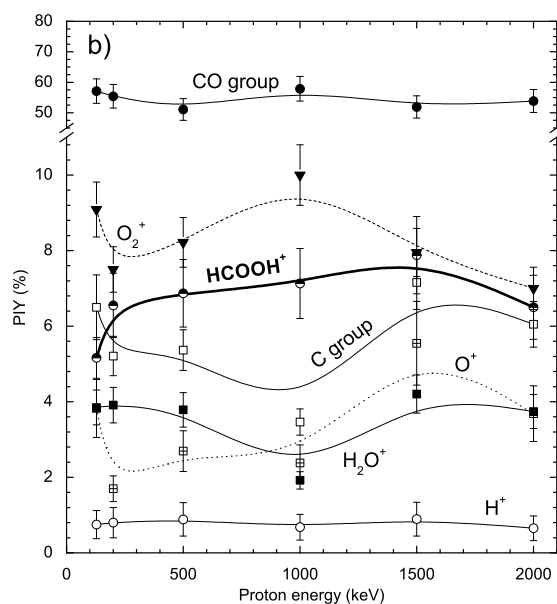
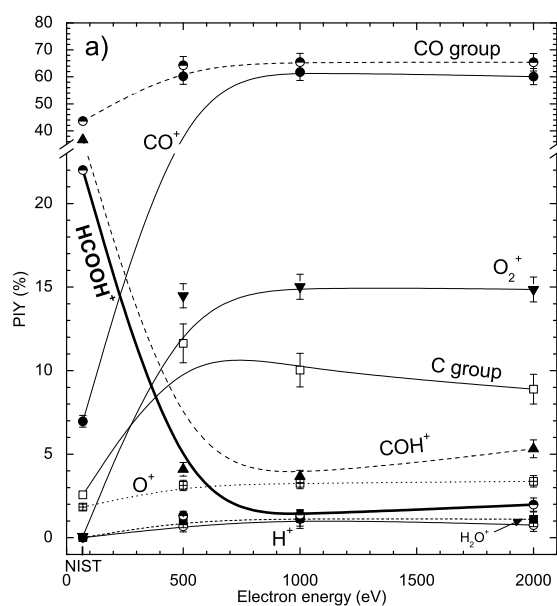


**Figure 5.** a) Comparison between partial ion yield (PIY) with 0.5 to 2 keV electron beam and b) 128 keV to 2 MeV proton beam.

the precise determination of  $\sigma_d$  of biomolecules is of paramount importance to estimate the molecular abundance in comets and in the interstellar medium. Moreover, knowing the particle flux and the  $\sigma_d$  value we can estimate the dissociation rate and the half-life of a specific molecule (Cottin et al. 2003; Bernstein et al. 2004).

It is well known that the cross sections for a given collision process related to the interaction of a fast projectile with a molecular target can be estimated by summing up all the separate cross sections of the constituent atoms of the molecule. Being generally difficult to endorse on theoretical bases, the additivity rule (i. e. the Bragg rule) is unremarkably the sole option available in the lack

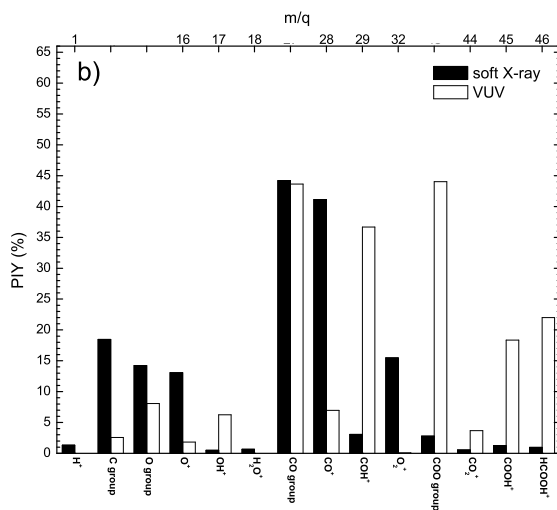
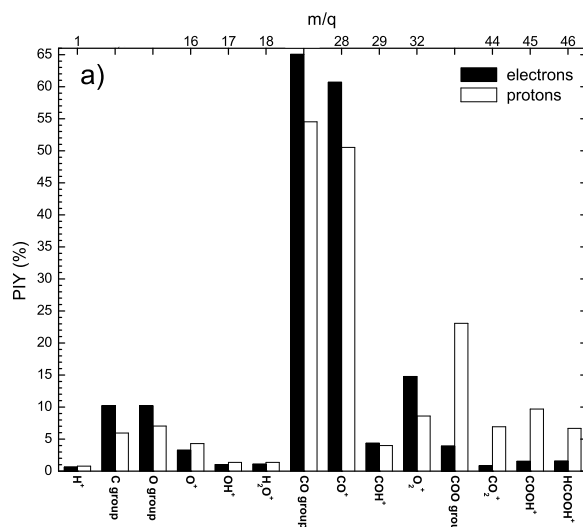


**Figure 6.** a) Comparison between partial ion yield (PIY) due dissociation with electrons beam (averaged between 0.5 to 2 keV) and a proton beam (averaged between 128 keV to 2 MeV). b) Comparison between partial ion yield (PIY) in soft X-ray field and VUV field from NIST 70 eV electron impact mass spectra (adapted from Boechat-Roberly, Pilling & Santos 2005).

of experimental ionisation cross section values for molecular targets. Adoption of this procedure is grounded on the premise that, for high projectile velocities, the target molecule operates as an assembly of separate atoms being its molecular nature negligible.

Watson et al. (2003) found that the total electron cross sections measured with a variety of molecular targets, when divided by the number of atoms per molecule and plotted versus target average atomic number, closely mirrored the straight-line  $Z^2$  dependence established by the cross sections for the atomic targets He and Ne. In the electron impact case, the additivity rule is also an undefeated approach (Mark & Dunn 1985; Bobeldijk et al. 1994; Miller 1990; Sun et al. 1998; Deutsch et al. 1996; Raj 1991; Joshipura & Patel 1994; Sun et al. 1994; Jiang, Sun & Wan, 1995a and 1995b).

The above mentioned observations mean that one can estimate

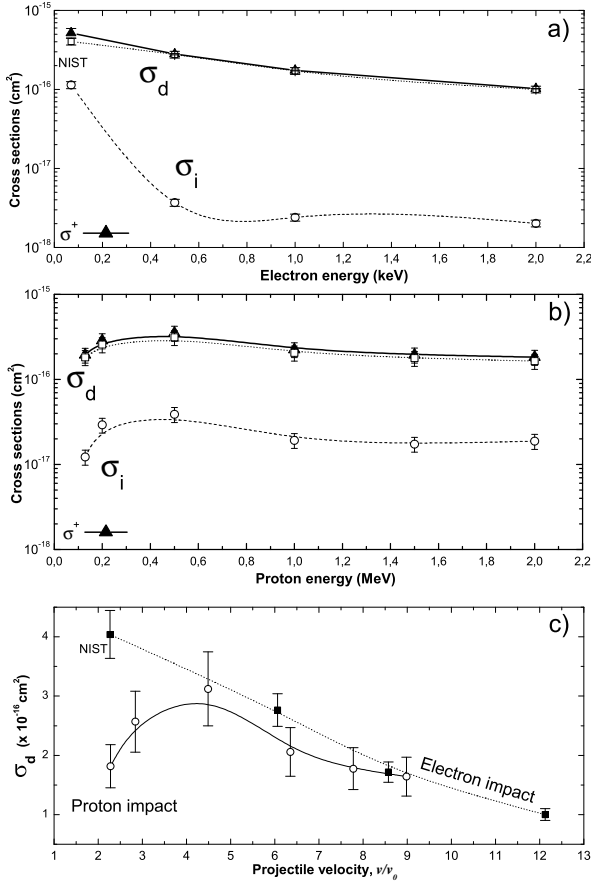


**Figure 7.** a) Total ion production cross section ( $\sigma^+$ ), non-dissociative single ionisation cross section ( $\sigma_i$ ) and dissociative ionisation cross section ( $\sigma_d$ ) of formic acid as a function of electron beam energy. b) The same for proton beam impact. c) Dissociation cross section of formic acid as a function of electron impact velocity ( $v/v_0 = \sqrt{E(eV)}/13.6$ ) and proton impact velocity ( $v/v_0 = 6.35 \sqrt{E(MeV)}$ ), for comparison. For the cross section of the 70 eV electron impact on HCOOH we used the PIY from NIST data base. See details in text.

the formic acid total ionisation cross sections  $\sigma_{HCOOH}^+$  by applying the additivity rule (ex.  $\sigma_{HCOOH}^+ = \sigma_{CO_2}^+ + \sigma_{H_2}^+$ ). In the electron impact case, we employed the averaged cross sections based on the theoretical calculations (Kim & Rudd 1994) for 70, 500, 1000 and 2000 eV electrons on ( $O_2 + CH_2$ ), ( $CO_2 + H_2$ ), ( $CO + H_2O$ ) and ( $CH + HO_2$ ). In the proton impact case, the cross section values introduced for the normalization procedure are the averaged cross sections based on the experimental determination (Rudd et al. 1985a and 1985b) for 1.0 MeV and 2.0 MeV protons ( $CO_2 + H_2$ ) and ( $CO + H_2O$ ). The cross sections used for the normalisation in this work are the average values of the summed pair of cross sections. In both proton and electron cases the calculated uncertainties are obtained from the chi-squared deviations.

The non-dissociative single ionisation (ionisation) cross section  $\sigma_i$  and the dissociative single ionisation (dissociation) cross section  $\sigma_d$  of formic by solar wind particles can be determined by

$$\sigma_i = \sigma^+ \frac{PIY_{HCOOH^+}}{100} \quad (5)$$

and

**Table 4.** Values of non-dissociative single ionization cross section ( $\sigma_i$ ) and dissociative ionization cross section ( $\sigma_d$ ) of formic acid as a function of electron impact energy. The estimated experimental error was below 30%.

Electron energy (keV)	Cross Sections (cm <sup>2</sup> )		
	$\sigma_d$	$\sigma_i$	$\sigma^+$
0.07 <sup>a</sup>	$4.04 \times 10^{-16}$	$1.14 \times 10^{-16}$	$5.18 \times 10^{-16}$
0.5	$2.76 \times 10^{-16}$	$3.69 \times 10^{-18}$	$2.80 \times 10^{-16}$
1.0	$1.72 \times 10^{-16}$	$2.40 \times 10^{-18}$	$1.74 \times 10^{-16}$
2.0	$1.00 \times 10^{-16}$	$2.02 \times 10^{-18}$	$1.02 \times 10^{-16}$

<sup>a</sup> PIY derived from NIST 70 eV electron impact mass spectra.

Proton energy (MeV)	Cross Sections (cm <sup>2</sup> )		
	$\sigma_d$	$\sigma_i$	$\sigma^+$
0.128	$1.82 \times 10^{-16}$	$1.23 \times 10^{-17}$	$1.94 \times 10^{-16}$
0.2	$2.57 \times 10^{-16}$	$2.92 \times 10^{-17}$	$2.86 \times 10^{-16}$
0.5	$3.13 \times 10^{-16}$	$3.89 \times 10^{-17}$	$3.51 \times 10^{-16}$
1.0	$2.06 \times 10^{-16}$	$1.93 \times 10^{-17}$	$2.25 \times 10^{-16}$
1.5	$1.78 \times 10^{-16}$	$1.74 \times 10^{-17}$	$1.95 \times 10^{-16}$
2.0	$1.64 \times 10^{-16}$	$1.88 \times 10^{-17}$	$1.83 \times 10^{-16}$

$$\sigma_d = \sigma^+ \left( 1 - \frac{PIY_{HCOOH^+}}{100} \right) \quad (6)$$

where  $\sigma^+$  is the cross section for single ionized fragments of HCOOH and  $PIY_{HCOOH^+}$  is the partial yield of formic acid ion in each impact case (see description in Boechat-Roberty, Pilling & Santos 2005).

Both cross sections are shown in Fig. 7, as a function of the projectile energy. In the upper panel, Fig. 7a, we display the total ionization cross section ( $\sigma^+$ ), the single ionization ( $\sigma_i$ ) and the dissociation cross section ( $\sigma_d$ ) of formic acid by energetic electron impact as a function of electron energy. For the 70 eV electron impact cross section we used the PIY from the NIST data base. In the middle panel, Fig. 7b, we exhibit the equivalent set of cross sections as a function of energetic particles impact velocity ( $v/v_0 = \sqrt{E(eV)}/13.6$  for electrons;  $v/v_0 = 6.35 \sqrt{E(MeV)}/m(a.m.u.)$  for ions) is presented in the lower panel, Fig. 7c.

The experimental values for the total ion production cross section ( $\sigma^+$ ), the non-dissociative single ionisation cross section ( $\sigma_i$ ) and dissociative ionisation cross section ( $\sigma_d$ ) of formic acid as a function of electron and proton impact energies are presented in Table 4. The estimated experimental error is considered to be lower than 30%

#### 4.4 Dissociation rate and half-life

The dissociation rate,  $R$ , of a molecule subjected to the interstellar/interplanetary particle field (ex. protons or electrons) in the energy range,  $\varepsilon_2 - \varepsilon_1$ , is given by

$$R = \int_{\varepsilon_1}^{\varepsilon_2} \sigma_d(\varepsilon) I(\varepsilon) d\varepsilon \quad (7)$$

where  $\sigma_d(\varepsilon)$  is the dissociation cross section as a function of projectile energy (cm<sup>2</sup>) and  $I(\varepsilon)$  is the particle flux as a function of energy (particles cm<sup>-2</sup> eV<sup>-1</sup> s<sup>-1</sup>).



**Table 5.** HCOOH Dissociation rate and half-life.

Dissociation source	Dissociation rate (1/s)	half-life (s)
Quiet sun at 1 AU (UV photons) <sup>a</sup>	$8.8 \times 10^{-4}$	$7.9 \times 10^2$
Quiet sun at 1 AU (UV photons) <sup>b</sup>	$3.2 \times 10^{-5}$	$2.1 \times 10^4$
Lyman $\alpha$ <sup>c</sup>	$3.9 \times 10^{-6}$	$1.7 \times 10^5$
Solar 0.07 - 2 keV electrons <sup>d</sup>	$9.8 \times 10^{-7}$	$7.1 \times 10^5$
Interstellar medium (theoretic) <sup>e</sup>	$6.7 \times 10^{-10}$	$1.0 \times 10^9$
Solar 0.1 - 2 MeV protons <sup>d</sup>	$5.7 \times 10^{-12}$	$1.2 \times 10^{11}$

<sup>a</sup> Huebner et al. 1992; <sup>b</sup> Crovisier 1994; <sup>c</sup> Suto et al. 1988;

<sup>d</sup> this work; <sup>e</sup> Roberge et al. 1991 (UV photons + cosmic rays).

From Eq. 7 we can also derive the half-life,  $t_{1/2}$ , of the molecule as

$$t_{1/2} = \frac{\ln 2}{\int_{\varepsilon_1}^{\varepsilon_2} \sigma_d(\varepsilon) I_0(\varepsilon) d\varepsilon} \quad (8)$$

which does not depend on the molecular number density.

A comparison between the dissociation rate and the half-life of the formic acid due to the interaction with UV photons (taken from literature) with the one determined from the interaction with energetic solar wind electrons and protons (this work), are presented in table 5.

From Table 5, we can see that the half-life for HCOOH due to both solar UV photons is about 1 order of magnitude lower than for the energetic electrons. However, as we can see in Fig. 1a, for the low energy electrons, the flux is about several orders of magnitude higher than for the energetic ones. This, combined with the fact that for small velocity electrons the dissociation cross section present an increase (see Fig. 7a and c), may promote values even higher in the dissociation rate for the small velocity electrons. These above statements, points out also the importance of the electron impact processes and data on chemical models.

Despite the similar fragmentation pattern in both cases, the interaction with fast protons seems to be less significant on the molecular cometary abundances. In fact, the determined half-life for the formic acid due to proton impact is about 4 thousand years, 6 order of magnitude higher than for the electron impact case.

## 5 CONCLUSIONS

The effects of energetic charged particles (protons and electrons), emanating from the solar wind, in the cometary gaseous formic acid molecule (HCOOH) have been reproduced in our laboratory. Absolute values for the ionisation and dissociation cross sections for the interaction of this molecule with solar wind particles (electrons and protons) have been determined. The energy range for the energetic electrons was 0.5 keV to 2 keV, and from 128 keV to 2 MeV for the fast protons.

In both cases mass spectra were obtained using time-of-flight mass spectrometry and coincidence techniques. In agreement with previous studies, the dissociation effects produced either by fast electrons or by soft X-rays have presented several similarities (Boechat-Roberty, Pilling & Santos 2005). The survival of HCOOH subjected to an incoming proton beam is found to be about 6-8% while in the fast electrons case it was about 2%, i.e., 3 to 4 times smaller. The reactive COOH<sup>+</sup> fragment, also important in pre-biotic ion-molecule chemistry, shows a behavior similar to the observed with the molecular ion HCOOH<sup>+</sup> in both cases.

The average dissociation cross section due to both energetic

projectiles, in the energy range studied, is approximately  $2 \times 10^{-16}$  cm<sup>2</sup>. However, a slight enhancement can be noted in the case of fast electrons impact. The non-dissociative single ionisation cross section present a value about 4-5 times higher in the case of energetic proton which can be associated with the slight enhancement in the total single ionization cross section due to proton impact when compared with the energetic electrons. Moreover, despite the fact that both projectiles lead to the same fragmentation pattern, we observed differences in the relative intensities of the ejected fragments.

The dissociation rates of formic acid due to UV photons and energetic electrons roughly in the same range of magnitude, despite the values for photons (from quiet sun) it at least 30 times larger than for fast electrons. This shows that, despite the interaction with solar wind particles studied here seems to be quite secondary compared to cometary photolytic processes, the electron impact processes should be taken into account on chemical models in an attempt to better simulate the interplanetary conditions. The above statement become critical, for example, in case of solar instabilities periods and if we consider the low energy (< 10 eV) electrons.

Given the fact that HCOOH is a minor cometary species, the studied process may have only a minor consequence on cometary chemistry, for example, in the production of the extended sources of CO or H<sub>2</sub>CO. However, this could be not the case for a much more abundant species such as methanol.

In the present work we have tried to contribute to the elucidation of questions involving the extended molecular sources in the cometary coma, such as the case of formaldehyde in the comet Halley (Meier et al. 1993), frequently associated with the dissociation process due to solar wind radiation. Based on our data, we expect for example, that some of the detected cometary CO could be the result of the dissociation processes of large molecules, as is the case of the formic acid. We hope that the molecular cross section derived in this work will give rise to more precise values for some molecular abundances in cometary coma models.

## ACKNOWLEDGMENTS

The authors would like to express their gratitude to MSc. F. C. Pontes. This work was supported by the Brazilian funding agencies FUJB (UFRJ), CAPES, CNPq, and FAPERJ.

## REFERENCES

- Bethe H., 1930, Ann. Physik 5, 325.
- Bernstein M. P., Ashbourn S. F. M., Sandford S. A. & Allamandola L. J., 2004, ApJ, 601, 365.
- Bobeldijk M., van der Zande W. J. & Kistemaker P. G., 1994, Chem. Phys. 179, 125.
- Boechat-Roberty H. M., Pilling S. & Santos A. C. F., 2005, A&A, 438, 915.
- Boice D. C., 2004, American Astronomical Society, DPS meeting 36, 25.04.
- Bockelée-Morvan D., Lis D. C., Wink J. E., Despois D., Crovisier J., et al., 2000, A&A, 353, 1101.
- Biver N., Bockelée-Morvan D., Boisser J., Colom P., Crovisier J., et al., 2005, IAU Symp. 291 - Asteroids, Comets and Meteorites, P5.1, pg. 43.
- Briscoe J. F. & Moore C. B., 1993, Meteoritics, 28, 330.
- Cravens T. E., 1997, Geophys. Res. Lett. 24, 105.

- Crovisier J., Bockelée-Morvan D., Colom P., Biver N., Despois D. & Lis D. C., 2004, *A&A*, 418, 1141.
- Crovisier J., 1994, *J. Geoph. Res. Planets* 99, 3777.
- Cottin H., Moore M. H. & Bénilan Y., 2003, *ApJ*, 590, 874.
- Deutsch H., Becker K., Pittner J., Koutecky V. B., Matt S. & Mark J. D., 1996, *J. Phys. B*, 29, 5175.
- D'Uston C., Reme H., Sauvaud J. A., Carlson C. W., Anderson K. A., Curtis D. W., Lin R. P., Korth A. & Mendis D. A., 1989, *Ann. Geophys.*, 7, 91.
- Ehrenfreund P. & Schutte W. A., 2000, *Ad. Space Res.*, 25, 2177.
- Fano U., 1954, *Phys. Rev.*, 95, 1198.
- Fuselier S. A., Shelley E. G., Goldstein B. E., Goldstein R., Neugebauer M., Ip W.-H., Balsiger H. & Reme H., 1991, *ApJ*, 379, 784.
- Goldstein B. E., Neugebauer M., Balsiger H., Drake J., Fuselier S. A., Goldstein R., Ip W. H., Rettenmund U., Schwenn R. & Shelley E. G., 1987, *A&A*, 187, 174.
- Gombosi T. I., 1987, *Geoph. Research Letters*, 14, 1174.
- Greenwood J. B., Smith S. J. & Chutjian A., 2000, *ApJ*, 529, 605.
- Grevesse N. & Sauval A. J., 1998, *Space Science Reviews*, v. 85, Issue 1/2, p. 161.
- Gringauz K. I., Gombosi T. I., Remizov A. P., Apathy I., Szemerey I., Verigin M. I., Denchikova L. I., et al., 1986, *Nature*, 321, 282.
- Häberli R. M., Altwegg K., Balsiger H. & Geiss J., 1995, *A&A*, 297, 881.
- Häberli R. M., Gombosi T. I., De Zeeuw D. L., Combi M. R. & Powell K. G., 1997, *Science*, 276, 939.
- Haider S. A. & Bhardwaj A., 2005, *Icarus*, 177, 196.
- Hansen, D. L. et al, 1998, *Phys. Rev. A*, 58, 5.
- Herbst E. & Leung C. M., 1986, *MNRAS*, 222, 689.
- Huebner W. F., Keady J. J. & Lyon S. P., 1992, *Astropys. Space Sci.*, 195, 1.
- Jiang Y. H., Sun J. F. & Wan L. D., 1995a, *Z. Phys. D: At., Mol. Clusters* 34, 29.
- Jiang Y. H., Sun J. F. & Wan L. D., 1995b, *Phys. Rev. A* 52, 398.
- Joshiyura K. N. & Patel P. M., 1994, *Z. Phys. D: At., Mol. Clusters* 29, 269.
- Kim Y.-K. & Rudd M. E., 1994, *Phys. Rev. A*, 50, 3954. See also at <http://physics.nist.gov/PhysRefData/Ionization/molTable.html>
- Krasnopolsky V. A., Greenwood J. B. & Stancil P. C., 2004, *Space Science Reviews*, 113, 271.
- Kroll N. A. & Trivelpiece A. W., 1973, "Principles of Plasma Physics", McGraw-Hill.
- Largo A., Redondo P. & Barrientos C., 2004, *Int. J. Quant. Chem.*, 98, 355.
- Lin R. P., McGuire R. E. & Anderson K. A., 1974, *IAU Symposium*, 57, 461.
- Liu S. Y., Girard J. M., Remijan A. & Snyder L. E., 2002, *ApJ*, 576, 255.
- Liu S. Y., Mehringer D. M. & Snyder L. E., 2001, *ApJ*, 552, 654.
- Maciel J. B., Morikawa E. & de Souza G. G. B., 1997, *Soc. Rad. Instr. AIP Conference Proceedings* 417, 22.
- Mark T. D. & Dunn G. H., 1985, "Electron Impact Ionization", Springer, New York.
- Meier R., Eberhardt P., Krankowsky D., Hodges R. R., 1993, *A&A*, 277, 677.
- Melo W. S., Santos A. C. F., Sant'Anna M. M., Sigaud G. M. & Montenegro E. C., 2002, *J. Phys. B: At. Mol. Opt. Phys.*, 35, L187.
- Miller K. J., 1990, *J. Am. Chem. Soc.* 112, 8533.
- Mumma M. J., Weissman P. R. & Stern S. A., 1993, "Comets and the Origin of the Solar System: Reading the Rosetta Stone", in *Protostars and Planets III*, E. H. Levy and J. I. Lunine, Eds., Univ. Arizona Press, Tucson, 1172-1252.
- Meier R., Eberhardt P., Krankowsky D., Hodges R. R., 1993, *A&A*, 277, 677.
- Mendoza, C., Ruetter, F., Martorell, G., & Rodríguez, L. S. 2004, *ApJ*, 601, L59.
- Ohishi M., Irvine W. M. & Kaifu N., 1992, *Astrochemistry of Cosmic Phenomena: edited by P. D. Singh*, Kluwer Academic Publishers, Dordrecht.
- Pilling S., Boechat-Roberly H. M., Baptista L. & Santos A. C. F., 2005, *IAU Symposium* 231.
- Pilling S., Santos A. C. F., Boechat-Roberly H. M., de Souza G. G. B., Sant'Anna M. M., Barros A. L. F., Wolff W. & de Castro Faria N. V., 2006, *Brazilian Journal of Physics*, 36, 538.
- Raj D., 1991, *Phys. Lett. A* 160, 571.
- Roberge W. G., Jones D., Lepp S. & Dalgarno A., 1991, *ApJS*, 77, 287.
- Rodgers S. D., Charnley S. B., Huebner W. F., Boice D. C., 2004, "Comets II", M. C. Festou, H. U. Keller, and H. A. Weaver (eds.), University of Arizona Press, Tucson, 745 pp., p.505-522
- Rodgers S. D. & Charnley S. B., 2001, *MNRAS*, 320, L61.
- Rudd M. E., Kim Y.-K., Madison D. H. & Gallagher J. W., 1985a, *Rev. Mod. Phys.*, 57, 4.
- Rudd M. E., Goffe T. V., DuBois R. D. & Toburen L. H., 1985b, *Phys. Rev. A*, 31, 492.
- Safronov V. S., 1969, "Evolution of the Protoplanetary Cloud and Formation of Earth and Planets", Nauka Press, Moscow (NASA TT-F-677).
- Santos A. C. F., Lucas C. A. & de Souza G. G. B. 2001, *J. Electron Spectrosc.*, 114, 115.
- Schwell, M., Dulieu, F., Jochims H. W. et al. 2002 *J. Phys. Chem A*, 106(45), 10908
- Shelley E. G., S. A. Fuselier, H. Balsiger, J. F. Drake, J. Geiss, B. E. Goldstein, R. Goldstein, W.-H. Ip, A. J. Lazarus & M. Neugebauer, 1987, *A&A*, 187, 304.
- Simon M., Lebrun T., Morin P., Lavollée M. & Maréchal L., 1991, *Nucl. Instrum. Methods*, B62, 167.
- Sorrell W. H., 2001, *ApJ*, 555, L129.
- Su H., Yong H. & Fanao K., 2000, *J. Chem. Phys.*, 113, Issue 5, 1891
- Sun J. F., Yu G. Q., Jiang Y. H. & Zhang S., 1998, *Eur. Phys. J. D* 4, 83.
- Sun J. F., Jiang Y. H. & L. D. Wan, 1994, *Phys. Lett. A* 195, 81.
- Suto M., Wang X. & Lee L. C., 1988, *J. Phys. Chem.*, 92, 3764
- Toptygin I. N., 1985, "Cosmic Rays in Interplanetary Magnetic Fields, Ed. B. M. McCormac", D. Reidel Publishing Company, Dordrecht, Holland
- Watson R. L., Peng Y., V Horvat, Kim G. J. & Olson R. E., 2003, *Phys. Rev. A*, 63, 2.
- Weissman P. R., 1991, "Dynamic History of the Oort Cloud", in R. L. Newburn, M. Neugebauer, and J. Rahe (Eds), *Comets in the Post-Halley Era*, Kluwer, Dordrecht, pg. 463-48.
- Winnewisser G. & Churchwell E., 1975, *Sterne und Weltraum*, 14, 288.
- Woon D. E., 2002, *ApJ*, 571, L177.
- Von Steiger R., Schwadron N. A., Fisk L. A., Geiss J., Gloeckler G., Hefli S., Wilken B., Wimmer-Schweingruber R. F. and Zurbuchen T. H., 2000, *J. Geophys. Res.*, 105, 27217.
- Young D. T., Crary F. J., Nordholt J. E., Bagenal F., Boice D., Burch J. L., Eviatar A., Goldstein R., et al., 2004, *Icarus*, 167, 80.
- Zuckermann B., Ball J. A. & Gottlieb A. C., 1971, *ApJ*, 163, L41.
- Zirin H., 1988, "Astrophysics of the Sun", Cambridge.

This paper has been typeset from a  $\text{T}_{\text{E}}\text{X}/\text{L}_{\text{A}}\text{T}_{\text{E}}\text{X}$  file prepared by the author.